Depolarization of optically pumped sodium atoms by wall surfaces

M. Tanaka
Kobe Tokiwa Jr. College, Ohtani-cho 2-6-2, Nagata Kobe 653, Japan

T. Ohshima and K. Katori
Laboratory of Nuclear Studies, Osaka University, Machikaneyama 1-1, Toyonaka Osaka 565, Japan

M. Fujiwara, T. Itahashi, H. Ogata, and M. Kondo
Research Center for Nuclear Physics, Osaka University, Mihogaoka 10-1, Ibaraki Osaka 567, Japan
(Received 31 August 1989)

The polarizations of sodium atoms optically pumped by a single-mode cw ring dye laser were measured as a function of the pumping power, sodium-vapor thickness, and external magnetic field for Pyrex glass and copper walls with and without dry-film coating. Observed quantities were analyzed by a simple optical pumping model in which the effect of the radiation trapping was taken into account. Assuming that the depolarization of the sodium atom was mainly induced by the local magnetic field at the sodium atom during its adsorption on the wall surface, the calculations could successfully reproduce the observed polarizations.

I. INTRODUCTION

Since Witteveen[1] and Anderson[2] first examined the possibility of polarized ion sources based on the spin-charge exchange collisions following the earlier work of Zavoiskii[3] and Haeberli,[4] the polarized proton sources[5-7] have been put to practical use by means of laser optical pumping of sodium atom. It has also been pointed out that the spin-charge exchange collisions are applicable to the polarization of other nuclei such as ^{3}He,[6,7]Li, and so on. On the basis of a wide variety of the applicability of the above method, we started constructing a polarized ^{3}He source as a first step of our project[8] in order to dedicate it to the cyclotron-cascade project of the Research Center for Nuclear Physics (RCNP), Osaka University, in which a $K=400$ MeV ring cyclotron has now been constructed.[9]

In the production of the nuclear polarization by the spin-charge exchange collisions, the large atomic polarization of sodium is indispensable to obtain the large nuclear polarization. The attainable maximum value of the atomic polarization optically pumped is mainly determined by the competition between pumping and depolarization rates. Possible origins of the depolarization have been rigorously discussed.[10-12] It has been found that the most serious depolarization is generated by the relaxation of the sodium atom during its adsorption on the wall surface of the sodium cell; in fact, an order of magnitude of the polarization changed with various surface materials. It was also inferred that the wall relaxation was caused by the local magnetic field during the time the sodium atom is adsorbed on the wall.

On the other hand, it has also been discussed that the effect of radiation trapping[13] is another source that decreases the polarization: A polarized sodium atom absorbs a photon emitted by a neighboring sodium atom optically pumped and eventually the final polarization is decreased. This effect becomes increasingly important as the sodium vapor thickness is increased. However, a few measurements[14] on this subject have been hitherto carried out only at a relatively low vapor thickness less than about 1×10^{13} atoms/cm^2. For practical use as a polarized ion source, a large sodium-vapor thickness is preferable because of the large efficiency of the spin-charge exchange collisions. Therefore, the investigation at the thicker sodium vapor thickness is necessary.

Based on the above aspects, our present work is concentrated on how the large atomic polarization of sodium can be obtained by optical pumping. For this purpose, we measured the sodium atomic polarization optically pumped by a single-mode cw ring dye laser at the sodium vapor thickness ranging from 4×10^{13} to 3×10^{14} atoms/cm^2 with various wall materials. The polarizations were measured as a function of the pumping laser power, sodium vapor thickness, and external magnetic field. We examined Pyrex glass and copper as suitable candidates for the wall materials at a typical operating temperature of around 500 K. To make the depolarization time longer we also tried Pyrex and copper walls coated with silicone, so-called "dry film."[10] A simple optical pumping model, in which the effect of the radiation trapping was taken into account, was applied to analyze the experimental results in terms of the depolarization mechanism.

The values of the polarization and sodium-vapor thickness were simultaneously measured by means of the Faraday rotation[15,16] as described in Sec. II. For this purpose, another broadband dye laser was used as probe laser light.

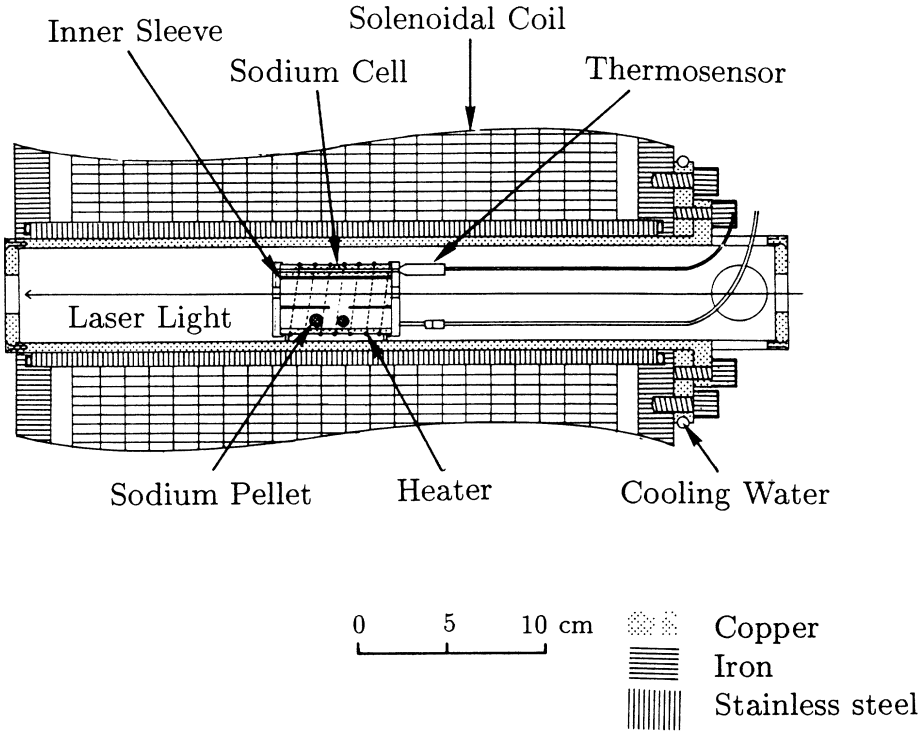

FIG. 1. Experimental setup of the polarization measurement.

II. EXPERIMENTAL PROCEDURE

A. Measurement of polarization

The Faraday rotation method was applied to measure the polarization and vapor thickness of sodium atoms; the plane of the polarization for the probe laser light is rotated when the light passes through the sodium vapor optically pumped in the presence of the external magnetic field. The rotation angle θ is approximated by

$$\theta=(\theta_0 B+\theta_P P)NL \ , \tag{2.1}$$

where B is the strength of the external magnetic field applied, N and L are the effective density and length of the sodium vapor, respectively, P is the polarization of sodium atoms, and θ_0 and θ_P are constants depending on the wavelength of the probe laser light which are numerically tabulated in Ref. 16. Using Eq. (2.1), we can determine not only the sodium-vapor thickness NL but the atomic polarization P of the sodium vapor in compliance with the following procedure. NL is obtained by comparing the rotation angle at $B=B_0$ with that at $B=0$ in the absence of the optical pumping ($P=0$). P is then obtained by comparing the rotation angle in the presence of the optical pumping with that in the absence of the optical pumping ($P=0$) at $B=B_0$.

Experimentally, the rotation angle could be determined by the intensity change of the probe laser light after passing through an polarization analyzer. In the present work, a Gran-Thomson prism was offered as follows. The polarization analyzer was rotated by an angle of $\pi/4$ rad relative to the plane of the polarization for the probe laser light incident on the sodium cell because the above angle setting was most sensitive to detect the rotation angle. Then the rotation angle θ is expressed by

$$\theta=\arcsin(I/2I_0)^{1/2}-\pi/4 \ , \tag{2.2}$$

where I_0 is an intensity of the incident probe laser light and I is an intensity of the probe laser light after passing through the polarization analyzer.

B. Sodium cell and surroundings

The experimental setup is shown in Fig. 1. A temperature-controlled sodium cell surrounded by a water-cooled copper baffle was inserted into a solenoidal coil. The inner sleeve (Pyrex glass or copper) of the sodium cell is designed to be replaceable. The length of the sodium cell was 6 cm. Sodium pellets were heated and vaporized. Through a hole in the inner sleeve the sodium vapor was introduced to the inner sleeve, where the sodium vapor was exposed in a pumping laser light. The strength of the magnetic field at the sodium cell generated by the solenoidal coil was changed from 0 up to 3 kG. Both sides of the cell have a hole with a diameter of 6 mm, through which pumping and probe laser lights are introduced. A 500-liter/sec diffusion pump and a 1800-liter/sec turbo molecular pump were located at both sides of the solenoidal coil for evacuation of the sodium vapor. The entrance and exit windows for the laser lights were made of wedge-shaped borosilicate glass to avoid the interference of the pumping laser light during its frequency scanning.

C. Laser system

Figure 2 shows a laser system, sodium cell, and block diagram of a data-taking system. Our laser system was composed of two sets of dye lasers using a Rhodamine 6G dye; a single-mode cw ring dye laser [380A, Spectra-Physics (SP) USA] for optical pumping and a broadband standing wave dye laser (375B, SP) for probing. Each of the dye lasers is pumped by a 5-W Ar-ion laser (168B, SP). These laser sets were stationed on a vibration-isolated table which was installed in a dried and dust-free room. The frequency of the ring dye laser for optical pumping was tuned to be in coincidence with the D_1 line of the sodium atom, i.e., 589.6 nm and that of the broadband dye laser was adjusted at 589.3 nm, which was just midway between the D_1 and D_2 lines of the sodium atom. The frequency broadening of the pumping and probe lasers was, respectively, ~ 1 MHz and ~ 10 GHz. The laser lights were then introduced to the sodium cell through optical mirrors. In order to convert the linear polarization to the circular one for the sake of optical pumping, a $\lambda/4$ plate was inserted in front of the entrance window. An emerging probe laser light from the sodium cell was guided to a Gran-Thomson prism. For monitoring an intensity of the probe laser light, a part of it was separated by a beam splitter in front of the Gran-Thomson prism.

D. Data taking

As shown in Fig. 2, a digital-to-analog–analog-to-digital converter (DAC-ADC) unit (PAD-1000S, Data Pro, Japan) is connected with a personal computer (PC9801VX, Fundamental Research Laboratories, NEC Corporation, Japan) via an RS232C communication line with a 9600 baude rate. The frequency of the pumping laser light was varied by a frequency scanner (481B, SP) controlled by an output signal of the DAC. If the Model 481B receives a DAC signal, then ADC1 and ADC2 accept output signals from a photomultiplier and a photodiode through DC amplifiers for the intensity measurements of the probe laser lights. The above process was repeated after each increment of the DAC output signal. Once the whole scanning was finished, all these ADC data were transferred to a floppy disk for an off-line analysis.

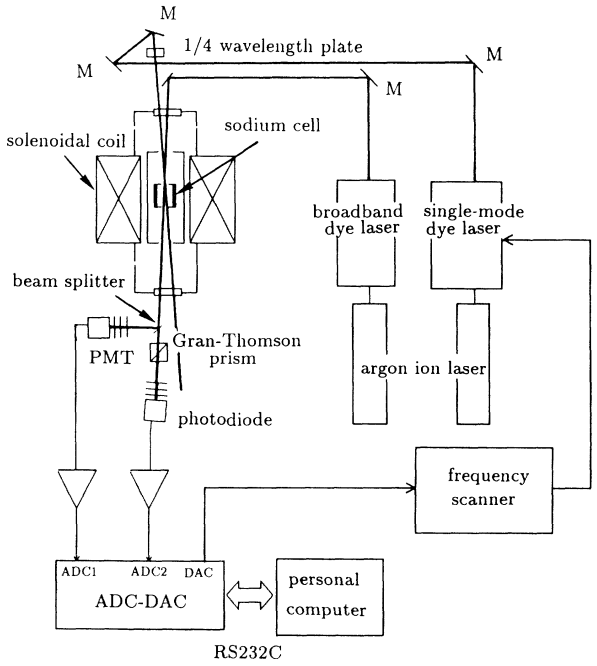

FIG. 2. Data taking system for the measurement of the sodium polarization.

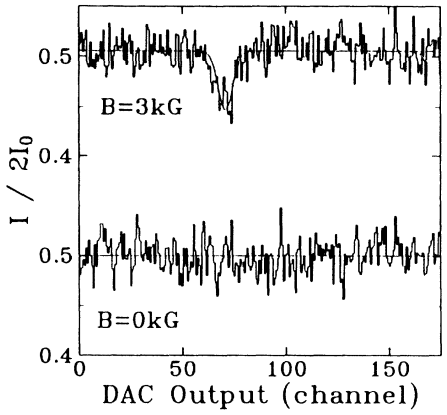

FIG. 3. Intensities of the probe laser light after passing through the Gran-Thomson prism are plotted as a function of the pumping laser frequency in the case of a copper wall. The upper curve was obtained with $B=3$ kG and the lower one was obtained with $B=0$ kG.

III. EXPERIMENTAL RESULTS

One of the frequency spectra taken for a copper wall is shown in Fig. 3, where the intensity of the probe laser light after passing through the Gran-Thomson prism is plotted as a function of the pumping laser light frequency in a range of 30 GHz. The upper and lower data correspond to the intensities measured under the conditions with B=3 and 0 kG, respectively. The dip shown in the upper figure obviously indicates the rotation of the plane of the polarization for the probe laser light, i.e., the occurrence of the atomic polarization as a result of optical pumping at the D_1 resonance frequency. The solid curves in the figure are the results of theoretical calculations assuming the Doppler line shape for the D_1 line with the hyperfine splitting. The absence of the dip in the lower figure indicates no polarization occurs. This suggests that the polarization depends on the external magnetic field. The *NL* value is deduced from the intensity difference between the lower and upper figures at the off-resonance region in Fig. 3. Then the polarization is deduced from the intensity difference observed for on- and off-resonance frequencies according to the procedure mentioned in Sec. II A.

Figure 4 shows the observed atomic polarizations of sodium for a Pyrex glass wall with and without dry-film

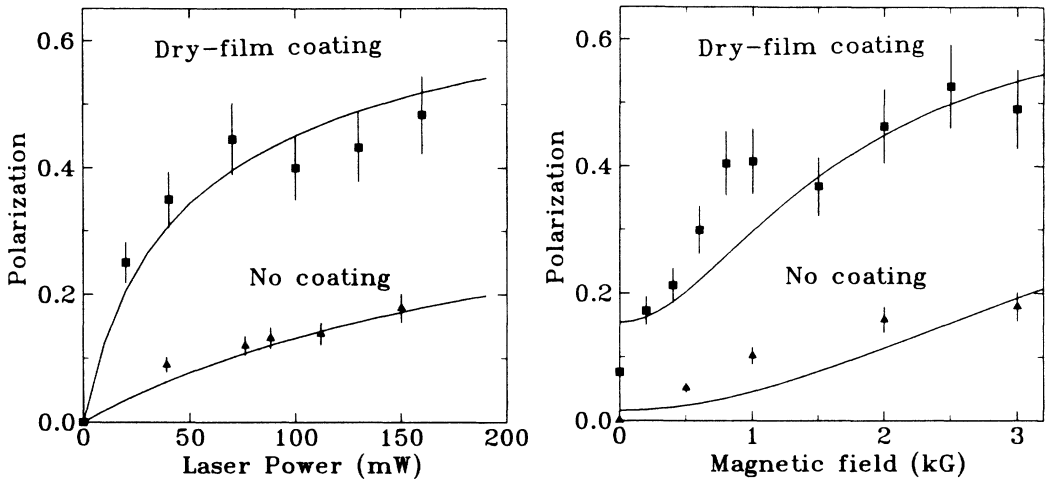

FIG. 4. The observed atomic polarizations of sodium are plotted for a Pyrex wall with and without dry-film coating at $NL \sim 4 \times 10^{13}$ atoms/cm^2. The left part shows a pumping laser power dependence obtained with $B = 3$ kG. The right part shows an external magnetic field dependence obtained with $I \sim 150$ mW. The solid curves in these figures are the results of the theoretical calculations (see text).

coating. Figure 5 also shows the observed atomic polarizations of sodium for a copper wall with and without dry-film coating. Each left part of Figs. 4 and 5 shows the results of the pumping laser power dependence and each right one the results of the external magnetic field dependence. The sodium-vapor thickness in the above measurements was $NL \sim 4 \times 10^{13}$ atoms/cm^2. In the polarization measurement on the laser power dependence the external magnetic field of 3 kG was applied, and on the magnetic field dependence the pumping laser power of 120–170 mW was applied. In Fig. 6, the observed atomic polarizations of sodium are plotted as a function of the sodium vapor thickness NL for dry-film-coated walls. In this measurement the external magnetic field of 3 kG and the pumping laser power of about 150 mW were applied. The error bars denoted in Figs. 4–6 are mainly due to the data fitting errors. The solid curves in these figures are the results of theoretical calculations. The detailed description of the calculations will be mentioned in the next chapter.

Above observations may be summarized as follows.

(i) The polarization increases according to both the pumping laser power and external magnetic field for all wall materials studied.

(ii) The polarization observed for walls coated with dry film enhances compared with those observed for walls without coating.

(iii) The polarization observed for the dry-film coated wall is comparable to one observed for the dry-film coated copper wall.

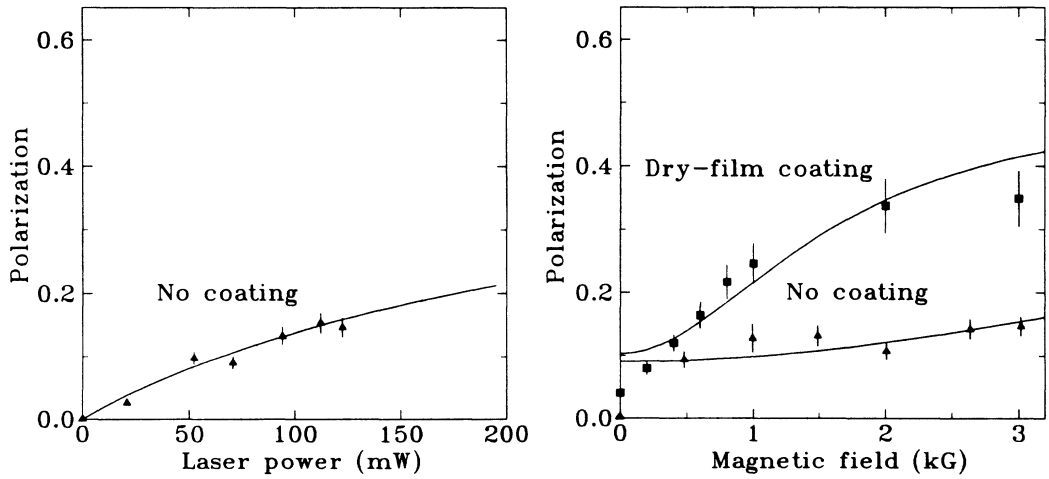

FIG. 5. The observed atomic polarizations of sodium are plotted for a copper wall with and without dry-film coating at $NL \sim 4 \times 10^{13}$ atoms/cm^2. The left part shows a pumping laser power dependence obtained with $B = 3$ kG only for a copper wall. The right part shows an external magnetic field dependence obtained with $I \sim 150$ mW. The solid curves in the figure are the results of the theoretical calculations (see text).

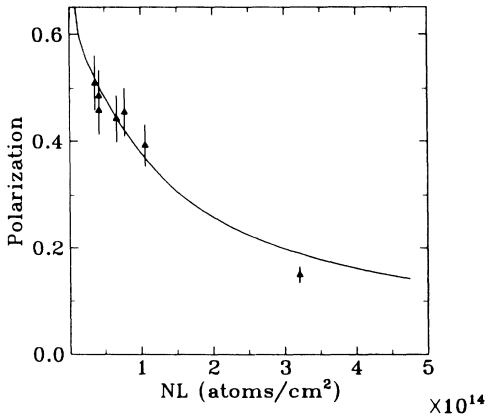

FIG. 6. The observed atomic polarizations of sodium are plotted for a dry-film-coating wall as a function of the sodium thickness NL. Here, the strength of the external magnetic field was 3 kG and the pumping laser intensity was ~150 mW.

(iv) The polarization is decreased by increasing NL.

These features demonstrate that the polarization is greatly influenced by the wall surface, the strength of the external magnetic field, and the sodium vapor thickness NL. This, in turn, suggests that the depolarization time T_1 is mainly determined by the surface conditions of the wall and the effect of the external magnetic field. In the following chapter the polarization will be calculated by using a simple optical-pumping model. The depolarization time due to the wall depolarization will be mentioned in detail.

IV. DISCUSSION

A. Optical pumping

A simple model calculation of optical pumping has been attempted to extract the atomic polarization of sodium. We assume that only the magnetic substates among the ground $3\,^2S_{1/2}$ and the first $3\,^2P_{1/2}$ excited state in the sodium atom take part in optical pumping disregarding the effect of the nuclear spin. For the sake of convenience we label the states as shown in Fig. 7: The

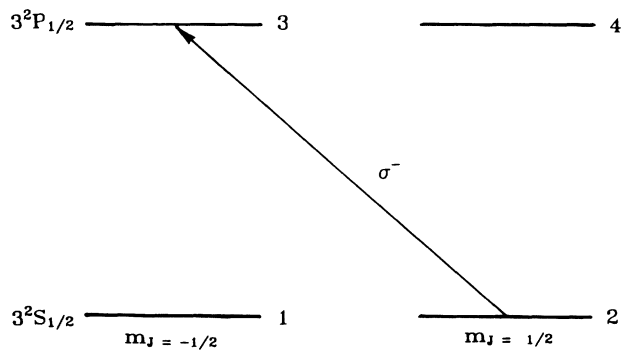

FIG. 7. Level scheme of the sodium atom. σ^- is a pumping light which induces the transition from the state labeled 2 to the state labeled 3.

$3\,^2S_{1/2}$, $m_J=-\frac{1}{2}$ state is labeled 1, the $3\,^2S_{1/2}$, $m_J=\frac{1}{2}$ state is labeled 2, the $3\,^2P_{1/2}$, $m_J=-\frac{1}{2}$ state is labeled 3, and the $3\,^2P_{1/2}$, $m_J=\frac{1}{2}$ state is labeled 4. If populations of the 1, 2, 3, and 4 states are written by n_1, n_2, n_3, and n_4, then the polarization P of the ground state of sodium atom is expressed by

$$P=-\frac{n_1-n_2}{n_1+n_2}\ . \tag{4.1}$$

Before going into a detailed discussion on the calculation of P, we must first remind ourselves of the following two experimental constraints.

(i) The diameter of the inner sleeve of the sodium cell (~15 mm) is larger than that of the pumping laser beam (~6 mm).

(ii) The frequency broadening of the pumping laser light (~1 MHz) is far smaller than that of sodium atoms, which is mainly determined by the broadening due to the Doppler effect (~1 GHz) plus the hyperfine splitting (1.7716 GHz).

The former effect will reduce the probability of optical pumping because the effective time of sodium atoms to be exposed in the pumping laser light is reduced by the thermal motion of sodium atoms. However, the multiple collisions of sodium atoms with the wall surface will recover a chance when sodium atoms intercept the pumping laser light. In the Appendix, an estimate of the reduction factor Q_w of the pumping rate due to the above effect will be presented, wherein the Monte Carlo calculation is employed. On the other side, the latter effect will also reduce the pumping probability because only a small portion of sodium atoms whose resonance frequency just coincides with the pumping laser frequency can be optically pumped. However, an enhancement of the pumping rate is expected because the velocity-changing collisions (VCC) of sodium atoms with the wall will help every sodium atom have a chance to fall into the laser light frequency region.[17] In other words, even if a single-mode dye laser light is used, it enables us to optically pump sodium atoms whose resonance frequencies are far broader than that of the laser light frequency. According to a simple estimate, the reduction factor of the pumping rate Q_f due to this effect is approximated by $\sim\Delta\omega_{\text{laser}}/\Delta\omega_{\text{Na}}=\frac{1}{3000}$, where $\Delta\omega_{\text{laser}}$ is a frequency broadening of the pumping laser light and $\Delta\omega_{\text{Na}}$ is a frequency broadening of the sodium atoms.

Taking those aspects into account, equations of optical pumping will be presented. Assuming the state 4 plays no role in optical pumping of the σ^--polarized light, P can be extracted by solving the rate equations involving the radiation trapping effect formulated by Tupa *et al.*[13] as given by

$$\frac{dn_1}{dt}=\frac{A_3}{3}n_3+\frac{n_2-n_1}{T_t}-\frac{A_3}{3}R_{31}(n_3,n_1)n_3\ , \tag{4.2}$$

$$\frac{dn_2}{dt}=-\alpha A_3(n_2-n_3)+\frac{2A_3}{3}n_3-\frac{n_2-n_1}{T_t}-\frac{2A_3}{3}R_{32}(n_3,n_2)n_3\ , \tag{4.3}$$

$$N=n_1+n_2+n_3 \ , \tag{4.4}$$

$$\alpha=\frac{\lambda_0^2}{4\pi}\frac{I_v}{h\nu}Q_wQ_fQ_a \ , \tag{4.5}$$

where N is a total number of atom, Q_a is the reduction factor of the incident laser light due to the light absorption by the sodium vapor, λ_0 is the D_1 resonance frequency, A_3 is the Einstein coefficient (6.1×10^7 sec^{-1} for sodium), T_t is a depolarization time between states 1 and 2, I_v is the intensity of the pumping laser per unit area of the light source, and $R_{31}(n_3,n_1)$ and $R_{32}(n_3,n_2)$ are the coefficients representing the effect of the radiation trapping. Here, the reduction factor Q_a is expressed in terms of an initial laser intensity I_0, the attenuation constant σ, and the sodium thickness NL by

$$Q_a=\frac{I_0}{\sigma NL}(1-e^{-\sigma NL}) \ . \tag{4.6}$$

We used the measured value of σ in the present work. The functional forms of $R_{31}(n_3,n_1)$ and $R_{32}(n_3,n_2)$ are given by

$$R_{31}(n_3,n_1)=K_1\frac{3}{2\sqrt{\pi}}\sum_i\omega_i\sum_j\omega_{3j}\left[\frac{1-\exp[-(n_1-n_3)R\gamma_iu_j]}{(1-u_j^2)^{1/2}}\right] , \tag{4.7}$$

$$R_{32}(n_3,n_2)=K_2\frac{3}{4\sqrt{\pi}}\sum_i\omega_i\sum_j\omega_{1j}\left[\frac{\left[1-\exp\left[-\gamma_i(n_2-n_3)\frac{2-u_j^2}{u_j}R\right]\right](2-u_j^2)}{(1-u_j^2)^{1/2}}\right] , \tag{4.8}$$

where K_1 and K_2 are constants to be determined so that $R_{31}(n_3,n_1)$ and $R_{32}(n_3,n_2)$ become unity when (n_1-n_3) and (n_2-n_3) are infinite, i.e., $K_1=1.1034$, $K_2=1.0541$,

$$\gamma_i=\frac{\lambda^2A_3}{8\pi}\left[\frac{MC^2}{2\pi kT\nu^2}\right]^{1/2}e^{-\chi_i^2} ,$$

χ_i and ω_i are the zeros and weighting factors of the Hermite polynomials, u_j and ω_{kj} are the zeros and weighting factors of the Gaussian polynomials,[18] and R is a diameter of an inner sleeve of the sodium cell. We solved above rate equations in compliance with Tanaka's formula,[19] which is an improved version of a Runge-Kutta method, initiating with the following conditions at $t=0$: $n_1=n_2=N/2$, $n_3=0$, and $\Delta t=0.5\times10^{-7}$. In Fig. 8, typical results of the calculated polarizations are shown as a function of the time for the following conditions: $NL=4\times10^{13}$ atoms/cm^2, the pumping laser power of 170 mW, and the depolarization time of 110 μsec. The calculations were carried out for cases in which the effect of the radiation trapping is switched on and off. From this result it is found that a considerable reduction of the polarization (20–30 %) occurs when the effect of the radiation trapping is switched on, suggesting that the effect of the radiation trapping should be taken into account at the sodium-vapor thickness of present interest.

B. Depolarization mechanism

Levy, Schmor, and Lalw[12] categorized the following possible depolarization mechanisms: (i) depolarization due to effusion of polarized atoms through entrance and exit holes of a sodium cell; (ii) depolarization due to collisions of polarized atoms with neighboring atoms; and (iii) depolarization induced by the local field felt by adsorbed sodium atoms on the wall surface of the inner sleeve of the sodium cell. According to their analysis, the former two criteria are not so important. In fact it is estimated that the depolarization time due to the effusion was ~300 μsec from the observation at the external magnetic field strong enough to decouple the local field caused by the effect shown in the third criterion. They also claimed that the second depolarization process is negligible at the vapor thickness of $\sim10^{13}$ atoms/cm^2.

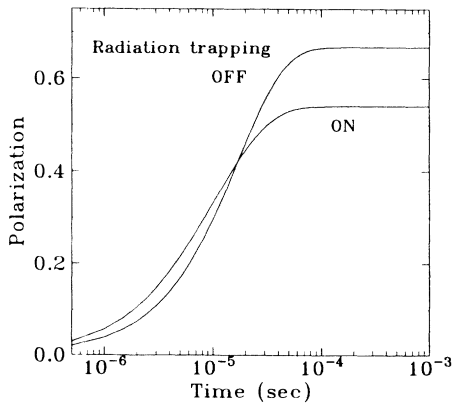

FIG. 8. Atomic polarizations of sodium are plotted as a function of the time for $NL=4\times10^{13}$ atoms/cm^2, the laser power of 170 mW, and the depolarization time of 110 μsec by solving the rate equations (see text). The calculations were carried out for both cases in which the effect of the radiation trapping is taken into account and not.

Consequently, the discussion hereafter is concentrated in the depolarization process categorized in the last criterion.

For this process there have been hitherto a few investigations since the pioneering work of Bouchiat and Brossel.[20] According to their analysis, the depolarization due to the wall surface is caused by the following processes. When an alkali atom strikes the wall, the van der Waals attraction force allows the atom to adsorb on the wall surface for a while and eventually the modulated magnetic fields generated by the motion of the atom on the wall surface will depolarize the atom. Here the effect of the electric quadrupole interactions on the depolarization of the alkali-metal atom can be disregarded because the atomic ground state with a spin of $\hbar/2$ has no terms corresponding to such interactions. The reciprocal of the depolarization time T_1^{-1} in an external magnetic field B is given by

$$T_1^{-1}=\frac{2}{3}\frac{\tau_s}{\tau_s+\tau_v}\gamma_s^2 b^2\tau_c\frac{1}{1+\left[\frac{eB}{m}\tau_c\right]^2}, \tag{4.9}$$

where eB/m is a Larmor frequency of the electron, τ_c is a correlation time for the modulation, τ_v is an average flight time between wall collisions (~ 10 μsec), τ_s is an average time that an atom remains on the surface at each wall collision $\gamma_s=g_e\mu_B/\hbar$, μ_B is the Bohr magneton, and b is a strength of a local magnetic field producing the depolarization. The correlation time τ_s is given by $1/\Gamma$, where Γ is the jumping rate of the adsorbed atoms on the surface which obeys the Arrhenius equation,[21]

$$\Gamma=\Gamma^0\exp(-E/kT), \tag{4.10}$$

where E denotes the diffusion energy and kT is the thermal energy. Bouchiat and Brossel[20] gave $\tau_s=1\times10^{-10}$ sec and $\tau_c=(0.4-1.5)\times10^{-10}$ sec. Levy, Schmor, and Lalw[12] discussed the depolarization mechanism assuming $\tau_s=\tau_c$ and extracted $\tau_c=0.84$ and 0.194×10^{-10} sec for a Pyrex and copper wall, respectively. To simplify our discussion, we used the values obtained by Levy, Schmor, and Lalw. The depolarization time due to effusion T_e was assumed to be 300 μsec from the result of the previous study.[12] Thus, the total depolarization time T_t to be inserted into Eqs. (4.2) and (4.3) is given in terms of T_1 and T_e as

$$T_t^{-1}=T_1^{-1}+T_e^{-1}. \tag{4.11}$$

Under this assumption, we carried out the calculations of the optical-pumping model using Eqs. (4.2)–(4.9) and (4.11). The solid curves in Figs. 4–6 are the calculated results wherein the strength of the local magnetic field b was given so that the calculations might reproduce the observed polarizations.

It is stressed that trends of the observed polarizations measured as a function of the pumping laser power, external magnetic field, and sodium-vapor thickness are consistently reproduced by the calculations with only one parameter, i.e., the strength of the local field b. This demonstrates that the model of optical pumping employed here exerts its validity. It is found that the strength of b was 0.4 kG for the dry-film-coated copper and Pyrex glass walls, 1.5 kG for the Pyrex glass wall, and 2.0 kG for the copper wall. These results are reasonably in agreement with the results of Levy, Schmor, and Lalw.[12]

V. CONCLUSION

We observed atomic polarizations of sodium using various wall surfaces of the inner sleeve of the sodium cell as a function of the pumping laser power, external magnetic field, and sodium-vapor thickness. It was found that "dry-film" coating and application of the external magnetic field more than 3 kG was indispensable to attain the polarization more than 0.5 with a relatively weak power of the pumping laser (~ 150 mW). From the optical-pumping model we succeeded in extracting the strengths of the local magnetic fields for any wall material studied and the deduced results were qualitatively in agreement with the results of the direct measurement of the depolarization time carried out by Levy, Schmor, and Lalw.[12]

ACKNOWLEDGMENTS

We express our sincere gratitude to Professor Y. Mori of the National Laboratory for High Energy Physics (KEK) for lending us a broadband dye laser and a 5-W Ar-ion laser. Our sincere thanks are also due to Professor D. Fick of Marburg/Max-Planck-Institut für Kernphysik, Heidelberg for his illuminating discussion on the depolarization mechanism caused by the wall surface. Sincere thanks are due to Professor T. Yamagata of Konan University and Professor H. Kimura of Osaka University for their hearty encouragement throughout this work. Thanks are also due to Dr. H. Okamura for his guidance in handling the laser. A part of this work has been supported by the Grant-in-Aid for General

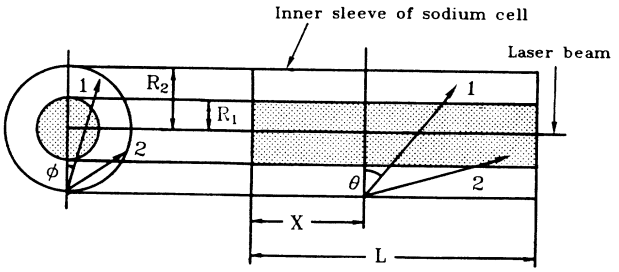

Trajectory 1: Sodium atom intercepts laser beam.
Trajectory 2: Sodium atom does not intercept laser beam

FIG. 9. Side and front views of the inner sleeve of the sodium cell. The sleeve has a cylindrical symmetry with respect to the laser light direction. The radius and length of the sleeve are R_2 and L, respectively. The laser beam line with the radius of R_1 is denoted by the dotted area. Trajectories of sodium atoms are labeled by 1 and 2. Trajectory 1 intercepts the laser beam and trajectory 2 does not intercept the laser beam. The starting position and the spatial direction of the sodium trajectory are denoted by X, θ, and ϕ, respectively.

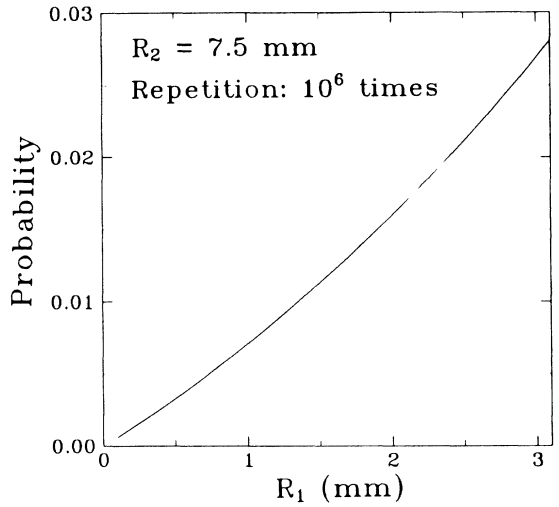

FIG. 10. The reduction rate of optical pumping caused by the condition that the radius of the inner sleeve of the sodium cell is larger than that of the pumping laser beam is plotted as a function of the radius of the laser by means of the Monte Carlo calculations.

Scientific Research of the Japanese Ministry of Education.

APPENDIX: AN ESTIMATE OF THE REDUCTION FACTOR OF OPTICAL PUMPING

In this Appendix we estimate the reduction factor of optical pumping caused by the reduction of the effective pumping time due to the thermal motion of sodium atoms in the inner sleeve of the sodium cell by means of the Monte Carlo calculations.

Suppose that the velocity of sodium atom is constant throughout every collision with the wall and the angular distribution of sodium atom emitted from the wall is isotropic. The emission angle of the sodium atom relative to the wall of the inner sleeve is defined as shown in Fig. 9, where R_1 and R_2 are the radius of the laser beam and the inner sleeve of the sodium cell, respectively, L is the total length of the sleeve, and x is the length measured from the left side of the wall. As shown in this figure, the sodium trajectory labeled 1 intercepts the laser beam in a definite range of θ,ϕ,x, while it has no chance to meet the laser beam as shown for the trajectory labeled 2. Thus, the intercepting length l_l for trajectory 1 through the laser beam is given by

$$l_l = 2R_2 \frac{\left[\left[\frac{R_1}{R_2}\right]^2 - \sin^2\phi\right]^{1/2}}{\cos\theta} , \tag{A1}$$

for $\phi \le \arcsin(R_1/R_2)$, $\theta \le \pi/2 - \arctan(R_2 - R_1/(L-x))$, and l_l for trajectory 2 is given by

$$l_l = 0 , \tag{A2}$$

for $\phi > \arcsin(R_1/R_2)$, $\theta > \pi/2 - \arctan(R_2 - R_1)/(L-x)$. On the other hand, the total length l_t of the sodium trajectory until the sodium atom reaches at the next wall is given by

$$l_t = \frac{2R_2\cos\phi}{\cos\theta} . \tag{A3}$$

A ratio of l_l to l_t corresponds to a fraction of the time for the sodium atom to stay in the laser beam during one collision. In order to obtain an average fraction of the time l_l/l_t, randomized numbers generated by a computer were given 10^6 times to x, θ, and ϕ in Eqs. (A1)–(A3), and l_l/l_t was calculated 10^6 times. Thus, the averaged value of l_l/l_t should be a reduction factor of optical pumping Q_w. In Fig. 10 Q_w is plotted as a function of a radius of the laser beam R_1, while $R_2 = 7.5$ mm and $L = 60$ mm.

[1]G. J. Witteveen, Nucl. Instrum. Methods **158**, 57 (1979).
[2]L. W. Anderson, Nucl. Instrum. Methods **167**, 363 (1979).
[3]E. K. Zavoiskii, Zh. Eksp. Teor. Fiz. **32**, 408 (1957) [Sov. Phys.—JETP **5**, 338 (1957)].
[4]W. Haeberli, in *Proceedings of the Second International Symposium on Polarization Phenomena of Nucleons, Karlsruhe, West Germany, 1965,* edited by P. Huber and H. Schopper (Birkhauser, Stuttgart, West Germany, 1966), p. 64.
[5]Y. Mori, A. Takagi, K. Ikegami, S. Fukumoto, and A. Ueno, J. Phys. Soc. Jpn. Suppl. **55**, 453 (1986).
[6]A. N. Zelenskii, S. A. Kokhanovski, V. M. Lobashev, and V. G. Polushkin, in *Proceedings of the Sixth International Symposium on Polarization Phenomena in Nuclear Physics, Osaka, 1985,* edited by M. Kondo, S. Kobayashi, M. Tanifuji, T. Yamazaki, K.-I. Kubo, and N. Onishi (Physical Society of Japan, 1986), p. 1064.
[7]L. Buchmann, C. D. P. Levy, M. McDonald, R. Ruegg, and P. W. Schmor (unpublished).
[8]M. Tanaka, T. Ohshima, K. Katori, M. Fujiwara, T. Itahashi, H. Ogata, and M. Kondo (unpublished).
[9]H. Ikegami (unpublished).
[10]D. R. Swenson and L. W. Anderson, Nucl. Instrum. Methods B **12**, 157 (1985).
[11]D. R. Swenson and L. W. Anderson, Nucl. Instrum. Methods B **29**, 627 (1988).
[12]C. D. P. Levy, P. Schmor, and W. M. Lalw, J. Appl. Phys. **63**, 4819 (1988).
[13]D. Tupa, L. W. Anderson, D. L. Huber, and J. E. Lawler, Phys. Rev. A **33**, 1045 (1986).
[14]Y. Mori, A. Takagi, K. Ikegami, S. Fukunaga, C. D. P. Levy, and P. W. Schmor, Nucl. Instrum. Methods A **268**, 270 (1988).
[15]W. D. Cornelius, D. J. Taylor, and R. L. York, Phys. Rev. Lett. **49**, 870 (1982).
[16]Y. Mori, K. Ikegami, A. Takagi, S. Fukumoto, and W. D. Cornelius, Nucl. Instrum. Methods **220**, 264 (1984).

[17]C. H. Holbrow, A. P. Ghosh, D. Heinzen, X. Zhu, W. W. Quivers, Jr., G. Shimkaveg, P. G. Pappas, J. E. Thomas, and M. S. Feld, Phys. Rev. A **34**, 2477 (1986).
[18]*Handbook of Mathematical Functions with Formulas, Graphs, and Mathematical Tables,* edited by M. Abramowitz and I. A. Stegun (Dover, New York, 1970), Chap. 7.
[19]S. Tanaka, dissertation, University of Tokyo, 1972.
[20]M. A. Bouchiat and J. Brossel, Phys. Rev. **147**, 41 (1966).
[21]B. Horn, W. Dreves, and D. Fick, Z. Phys. B **48**, 335 (1982).

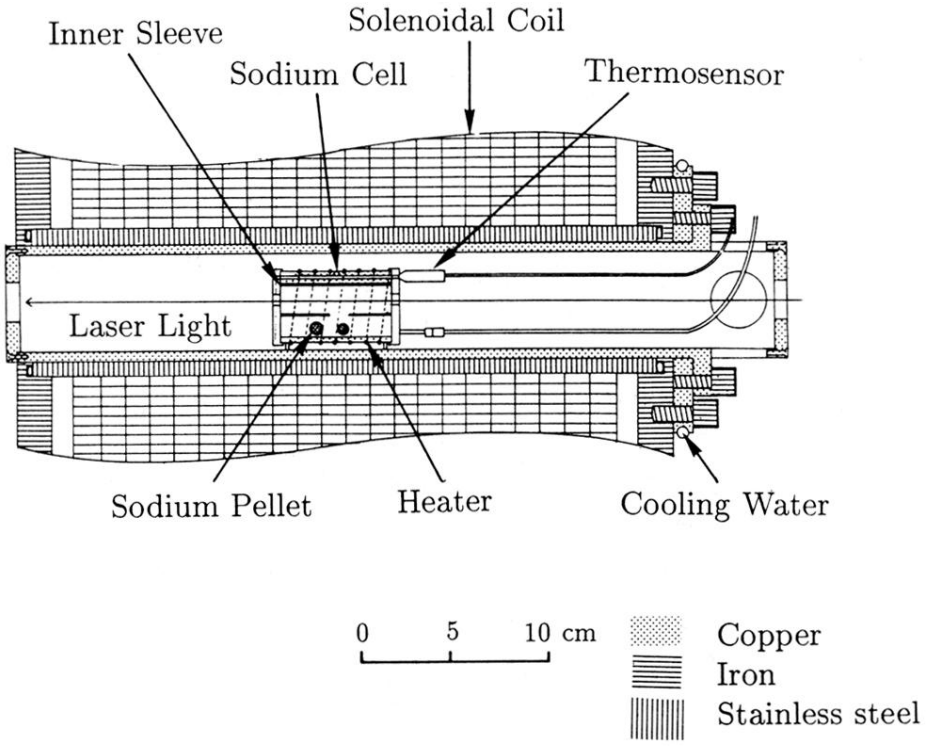

FIG. 1. Experimental setup of the polarization measurement.

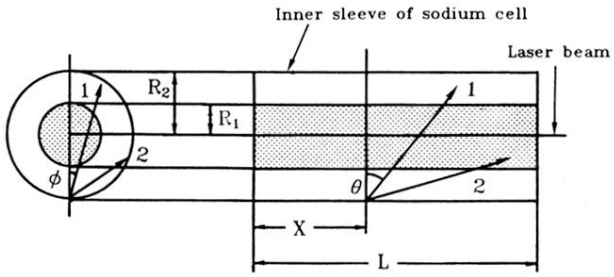

Trajectory 1: Sodium atom intercepts laser beam.
Trajectory 2: Sodium atom does not intercept laser beam

FIG. 9. Side and front views of the inner sleeve of the sodium cell. The sleeve has a cylindrical symmetry with respect to the laser light direction. The radius and length of the sleeve are R_2 and L, respectively. The laser beam line with the radius of R_1 is denoted by the dotted area. Trajectories of sodium atoms are labeled by 1 and 2. Trajectory 1 intercepts the laser beam and trajectory 2 does not intercept the laser beam. The starting position and the spatial direction of the sodium trajectory are denoted by X, θ, and ϕ, respectively.